On the spacing of Langmuir circulation in strong shear

By W. R. C. PHILLIPS

Department of Theoretical and Applied Mechanics, University of Illinois
at Urbana-Champaign, Urbana, IL 61801-2935, USA
wrphilli@uiuc.edu

The inviscid instability of $O(\epsilon)$ two-dimensional free-surface gravity waves propagating along an $O(1)$ parallel shear flow is considered. The modes of instability involve spanwise-periodic longitudinal vortices resembling oceanic Langmuir circulation. Here, not only are wave-induced mean effects important but also wave modulation, caused by velocity anomalies which develop in the streamwise direction. The former are described by a generalized Lagrangian-mean formulation and the latter by a modified Rayleigh equation. Since both effects are essential, the instability may be called 'generalized' Craik–Leibovich (CLg). Of specific interest is whether spanwise distortion of the wave field, both at the free surface and in the interior, acts to enhance or inhibit instability to longitudinal vortices. Also of interest is whether the instability gives rise to a preferred spacing for the vortices and whether that spacing concurs well or poorly with experiment. The layer depth is varied from much less than the e-folding depth of the $O(\epsilon)$ wave motion to infinity. Relative to an identical shear flow with rigid though wavy top boundary, it is found, *inter alia*, that wave modulation acts in concert with the free surface, at some wavenumbers, to increase the maximum growth rate of the instability. Indeed, two preferred spanwise spacings occur, one which gives rise to longitudinal vortices through a convective oscillatory bifurcation and a second, at higher wavenumber and growth rate, through a stationary bifurcation. The preferred spacings set by the stationary bifurcation concur well with those observed in laboratory experiments, with the implication that the instability acting in the experiments is very likely to be CLg.

1. Introduction

Mariners have long observed froth-marked rows on the ocean surface that more or less align with the wind, but their cause remained in question until Langmuir (1938) realized they are surface manifestations of counter-rotating rolls in the ocean beneath. Now known as Langmuir circulation, or LC, their spacings range from millimetres to several hundreds of metres and rule of thumb observations suggest they form in the presence of surface waves tens of minutes after the onset of winds above 3 m s^{-1} often, although not always, in conjunction with wave breaking. Of the suggested models to explain LC, the most plausible have as their basis an inviscid instability arising from the nonlinear interaction between surface gravity waves and wind-induced shear flow, the prevailing theory being that of Craik & Leibovich (1976). This theory assumes irrotational surface waves of slope $\epsilon \ll 1$, which act through their Stokes drift (an $O(\epsilon^2)$ averaged quadratic nonlinearity) on an $O(\epsilon^2)$ shear flow (see below

for a physical description). Two instability mechanisms, denoted CL1 and CL2, arise within this framework according to whether the Stokes drift or shear are cross-wind dependent or independent.

CL2 is thought more relevant in the open ocean because it acts in a wave field without special spatial structure. But in spite of its widespread acceptance (Thorpe 2004), and although it is known to capture some features of ocean LC (Phillips 2001*b*, 2002), evidence that LC are in fact excited by CL2 is at best circumstantial, and in order to support or negate CL2's relevance, attention turned to the laboratory. In this vein Melville, Shear & Veron (1998) and Veron & Melville (2001) conducted a series of careful experiments designed to excite LC in an environment as well controlled as possible. Specifically, they conducted their experiment in a wind-wave tank sufficiently long, wide and deep to minimize end effects; chose neutrally stratified conditions to exclude internal waves and thermal effects; and restricted attention to an essentially laminar environment to minimize the role of turbulence.

When the free surface of quiescent water in the experiments is subjected to an air flow it first undergoes shear, after which wind waves form and ultimately LC. But although the wave slope concurs with that in CL2-theory, effects of scale necessitate that the shear (defined below) in the experiment be $O(1)$, rather than the $O(\epsilon^2)$ level assumed in CL2, thereby excluding a one-to-one comparison. However such a comparison is possible with Craik's (1982) more general CLg-theory, which allows for all levels of shear in the presence of $O(\epsilon)$ rotational waves.

Craik considers two-dimensional monochromatic straight-crested waves of phase velocity $\mathscr{C}$ on, and parallel to, a unidirectional mean shear flow of characteristic velocity $\mathscr{V}$. Since orbital velocities in the wave field are characterized by $\epsilon\mathscr{C}$, the two velocity scales are related as $\mathscr{V}/\mathscr{C} = O(\epsilon^s)$, where $s \geqslant 0$. Furthermore, if variables are rendered dimensionless with respect to $\mathscr{C}$ and $\mathscr{L}$, where $\mathscr{L}$ is the characteristic thickness of the shear layer, the level of shear is also $O(\epsilon^s)$. Craik developed the theory for inviscid flow and considers $s = 0$, 1 and 2; Phillips (1998) later extended the theory to account for viscous effects, arbitrary $s \geqslant 0$ and a spectrum of waves.

Our intent here is to mimic the aforementioned laboratory experiments by studying the instability to CLg of inviscid $O(\epsilon)$ two-dimensional free-surface gravity waves propagating along an $O(1)$ parallel shear flow. But before proceeding it is important to realize that CLg and CL2 have fundamental differences, even though differential drift (see below) and shear are mandatory to both. Specifically, while CLg is wave catalysed, its relative CL2 is wave driven (McIntyre & Norton 1990). This means, *inter alia*, that the magnitude of velocity perturbations associated with each instability can differ significantly: indeed, while those in CL2 are uniformly bound by $O(\epsilon^2)$, their counterparts in CLg are determined by the magnitude of the pre-existing vorticity in the initial state, namely $O(\epsilon^s)$. In consequence velocity perturbations associated with CLg can be large enough to modulate the wave field. This means that CLg-theory must allow not just for the effects of the waves on the mean flow, but also the back effect of instability-induced velocity perturbations on the waves.

Physically, differential drift causes vortex lines (which move with the fluid) to tilt streamwise wherever the mean shear is laterally (i.e. cross-wind) distorted, giving rise to a streamwise component of vorticity and ultimately vortices. This is so in both CL2 and CLg. But while the drift remains cross-stream independent in CL2, wave modulation renders it cross-stream dependent in CLg, thereby affecting the degree to which vortex lines are tilted and the severity of the instability. The severity is

further affected by boundary conditions which in turn determine where modulation is a maximum. For example rigid wavy walls relegate the maximum to the interior where it acts to diminish the instability, whereas the maximum occurs at the boundary when the boundary is a free surface. This acts to enhance the instability, but only at some wavenumbers; indeed it allows the instability to tune to a maximum at specific wavenumbers, thereby introducing a preferred spacing for the modulation, streamwise velocity perturbation and the Langmuir circulation.

Craik (1982) and Phillips (1998) employ Andrews & McIntyre's (1978) generalized Lagrangian mean (GLM) equations to formulate CLg-theory. Herein the Lagrangian mean velocity is the sum of the Eulerian mean velocity and the generalized drift, while wave–wave and wave–shear interactions are captured in two averaged quadratic nonlinearities, the generalized drift and the pseudomomentum. Craik and Phillips use the GLM equations because they are canonical as an avenue to elucidate structure in wavy shear flows (see §2), particularly when the waves are rotational. But the GLM equations cannot in turn describe the back effect of flow anomalies on the waves; to do so the Euler equation (E) must be employed without averaging in a concurrent calculation. Of course in the absence of wave modulation and with $s = 2$, the CLg-equations recover the CL-equations of Craik & Leibovich (1976).

Studies of CLg in $O(1)$ shear bounded by rigid wavy walls indicate that wave modulation acts to diminish and in some instances thwart the instability (Phillips & Wu 1994, henceforth referred to as PW). Comparisons with experiments by Gong, Taylor & Dörnbrack (1996) further indicate that CLg is physically realizable (Phillips, Wu & Lumley 1996). But unlike CL2, where instability is assured in a neutral wavy disturbance only when differential drift and shear are of the same sense (for temporal wavy disturbances see Phillips 2002, 2003), instability to CLg must satisfy the necessary but not sufficient Craik–Phillips–Shen criterion (Craik 1982; Phillips & Shen 1996). This criterion states that an $O(1)$ shear flow bounded by rigid wavy walls is unstable to CLg if, from the reference frame of the waves and in the direction of increasing mean shear, the relative increase in mean velocity exceeds the relative increase in wave amplitude; specifically (in terms of later defined variables), $\vartheta \, \mathrm{d}U/\mathrm{d}z > U \, \mathrm{d}\vartheta/\mathrm{d}z$ where $\vartheta = \alpha|\Phi|$. But unclear is: (i) whether the Craik–Phillips–Shen criterion holds for $O(1)$ shear flows bounded by a free surface; and (ii) whether CLg can capture features of Melville *et al.*'s and Veron & Melville's experiments, specifically the cross-wind spacing of the LC at onset.

Our intent is to address these questions. In order to do so we revisit the work of PW, and in particular a case they study of $O(1)$ shear beneath surface gravity waves. However we shall not, as they did, restrict attention to a parameter range in which wave modulation and velocity perturbations are inhibited at the free surface; here both may occur. We find that such deformations act not only to enhance the instability (relative to its rigid walled counterpart) but also introduce a preferred spacing at which vortices form. This spacing concurs well with that observed by Melville *et al.* and Veron & Melville, with the implication that the instability acting in their experiments is very likely to be CLg.

Our study considers LC in water of both finite and infinite depth. We begin in §2 with an outline of Craik's eigenvalue problem for CLg. The free-surface boundary conditions are derived in §3, followed by a description of the numerical procedure employed (in §4). Our primary velocity and wave fields are detailed in §5. Finally, our results are given in §6, compared to experiment in §7 and discussed in §8.

2. Formulation

Andrews & McIntyre's GLM formulation is an exact theory of nonlinear waves on a Lagrangian-mean flow, which preserves the inviscid conservative properties of the E equation when the waves are rotational. To express ideas like steady mean flow, an Eulerian description of the Lagrangian mean, with position x and time t as independent variables, is employed. Hence the GLM description is really a hybrid Eulerian–Lagrangian description of wave mean-flow interactions. In consequence GLM and E may be used concurrently in an analysis which involves both averaged and non-averaged quantities, subject to the caveat that the mapping between the true Lagrangian and the reference GLM be smooth and invertible with a continuous inverse (i.e. a diffeomorphism). The average may be temporal, spatial or ensemble as befits the problem under consideration.

Craik (1982) and Phillips (1998) employed GLM and E equations to study a class of unidirectional wavy shear flows which bifurcate to longitudinal vortex motions via CLg. Herein the timescale over which the vortices evolve is long with respect to the wave period, so appropriate averages for GLM are: a temporal average over the wave period or a longitudinal spatial average over one wavelength. Craik restricted attention to inviscid shear flow with imposed neutral waves, while Phillips allowed for temporal viscous flow and growing waves. In their most general form, the disturbance equations, in conjunction with an energy equation given by Phillips (2002), yield the CLg equations.

2.1. *Craik's eigenvalue problem*

Here we restrict attention to spanwise-independent neutral free-surface gravity waves propagating along an $O(1)$ parallel shear flow and, as noted in §1, normalize with respect to $\mathscr{L}$ and $\mathscr{C}$. Then with space coordinates (x, y, z), unit vectors (i, j, k) and with an Eulerian-mean velocity profile $U(z)$ in $[z_a, z_b]$, our primary shear flow in a reference frame that moves in the x-direction with the phase speed of the waves is $[\bar{U}(z), 0, 0]$, where $\bar{U} = U(z) - 1$. However to ensure the mapping to GLM remains invertible we must exclude critical layers by requiring $\bar{U} \neq 0$. For clarity, upper-case letters are used to denote primary flow quantities, which by design are devoid of spanwise (y) dependence, with lower-case letters otherwise.

2.1.1. *From GLM*

Our expectation is that the wave/mean-flow interaction satisfies the Craik–Phillips–Shen criterion and is thus susceptible to the CLg instability. So, in view of work by Craik (1982) and Phillips (1998) who show that the cross-stream velocity perturbations are a factor ϵ smaller than the streamwise component when the shear is $O(1)$, we envisage small spanwise-periodic perturbations with streamwise-averaged Eulerian velocity components $(\tilde{u}, \tilde{v}, \tilde{w})$ of the form

$$(\tilde{u}, \tilde{v}, \tilde{w}) = \Delta \mathrm{Re}\{\mathrm{e}^{\sigma t}\mathrm{e}^{\mathrm{i}ly}[\hat{u}(z), -\epsilon\mathrm{i}\hat{v}(z), \epsilon\hat{w}(z)]\}, \tag{2.1}$$

which, correct to $O(\epsilon^2)$, satisfy continuity as $l\hat{v} + \hat{w}' = 0$ (see McIntyre 1988). Here Δ is a second small parameter that measures the strength of this motion relative to the primary shear flow, while σ is the growth rate of the motion and l is its spanwise wavenumber.

Commensurate with (2.1), wave modulation is necessarily largest in the streamwise direction. So, because that modulation is reflected in the pseudomomentum p (an averaged quadratic wave–wave nonlinearity) which is an $O(\epsilon^2)$ quantity, streamwise

distortion to it is $O(\epsilon^2 \Delta)$, so we expand its streamwise component p as

$$p = \epsilon^2 P + \epsilon^2 \Delta \mathrm{Re}\{e^{\sigma t} e^{ily} \hat{p}(z)\} + O(\epsilon^4, \epsilon^3 \Delta, \epsilon^2 \Delta^2). \tag{2.2}$$

Here P is the component which arises from the primary wave field, while $\mathrm{Re}\{e^{ily} \hat{p}\}$ is the spanwise-periodic perturbation arising from wave modulation.

Then substituting (2.1) and (2.2) into the GLM or CLg equations for an $O(1)$ shear flow and using continuity, yields at $O(\epsilon \Delta)$

$$\sigma_1 \hat{u} = -\hat{w} \bar{U}' \quad \text{and} \quad \hat{w}'' + l^2 \left[\frac{P' \bar{U}'}{\sigma_1^2} - 1 \right] \hat{w} = -\frac{l^2 \bar{U}'}{\sigma_1} \hat{p}, \tag{2.3a, b}$$

where $\bar{U}$ and l are specified, $\sigma = \epsilon \sigma_1$ is unknown and a prime denotes $\mathrm{d}/\mathrm{d}z$.

In order to determine P and $\hat{p}$, however, we require knowledge of the imposed wave field, and for that we refer to E (see §2.1.2). Craik (1982) and Phillips (1998) give details for obtaining both P and $\hat{p}$ in monochromatic wave fields, while Phillips (2001a) gives details to determine P for discrete and continuous spectra of waves.

2.1.2. *From E*

Calculation of the averaged quadratic nonlinearity $\hat{p}$ is in two parts: in the first we forgo averaging and calculate modulation to the x-periodic wave field due to the $O(\Delta)$ streamwise velocity perturbation $\tilde{u}$; we then employ that information within the construct of GLM. Further, because wave modulation is due primarily to $\tilde{u}$, we consider only the linear theory of wave motion in the presence of our mean Eulerian flow $\bar{U} + \tilde{u}$. So, since the waves are $O(\epsilon)$ and distortion to them is $O(\epsilon \Delta)$, we assume an x-periodic wave field $\breve{u}$ of the form

$$\breve{u} = \epsilon \mathrm{Re}\{e^{i\alpha x}[\Phi'(z), 0, -i\alpha \Phi(z)]\}$$
$$+ \epsilon \Delta \mathrm{Re}\{e^{\sigma t} e^{i\alpha x}[\mathrm{ɥ}(z) \cos ly, \mathrm{ɣ}(z) \sin ly, \mathrm{ɯ}(z) \cos ly]\} + O(\epsilon^2, \epsilon \Delta^2). \tag{2.4}$$

Since (2.4) is necessarily a solution to E we find, at $O(\epsilon)$, that $\Phi(z)$ and the streamwise wavenumber α must together satisfy the Rayleigh equation,

$$\bar{U}(\Phi'' - \alpha^2 \Phi) - \bar{U}'' \Phi = 0. \tag{2.5}$$

It then follows, with information from GLM, that the primary pseudomomentum is (Craik 1982)

$$P = -\frac{\bar{U}}{2} \left\{ \left| \left(\frac{\Phi}{\bar{U}} \right)' \right|^2 + \alpha^2 \left| \frac{\Phi}{\bar{U}} \right|^2 \right\}. \tag{2.6}$$

The velocity components $\mathrm{ɥ}$, $\mathrm{ɣ}$ and $\mathrm{ɯ}$ on the other hand, derive from modification of the $O(\epsilon)$ wave field by the $O(\Delta)$ spanwise-periodic component $\tilde{u}$ and satisfy continuity through $i\alpha \mathrm{ɥ} + l\mathrm{ɣ} + \mathrm{ɯ}' = 0$. But to evaluate them we need a counterpart to Φ and (2.5) at $O(\epsilon \Delta)$. We thus introduce $\hat{\phi}(z) = i\alpha^{-1} \mathrm{ɯ}(z)$ and employ continuity with E to obtain the Rayleigh–Craik equation (Craik 1982),

$$\bar{U}[\hat{\phi}'' - (\alpha^2 + l^2)\hat{\phi}] - \bar{U}'' \hat{\phi} = -\hat{u}[\Phi'' - (\alpha^2 + l^2)\Phi] + \hat{u}'' \Phi. \tag{2.7}$$

Finally, with information from GLM, and after considerable algebra, we obtain the averaged quadratic nonlinearity $\hat{p}$ as

$$\hat{p} = \mathbb{A}(z)\hat{u}(z) + \mathbb{B}(z)\hat{u}'(z) + \mathrm{Re}\{\mathbb{C}(z)\hat{\phi}(z) + \mathbb{D}(z)\hat{\phi}'(z)\}, \tag{2.8}$$

where $\mathbb{A}$, $\mathbb{B}$, $\mathbb{C}$ and $\mathbb{D}$ are z-dependent functions which are independent of σ_1:

$$\mathbb{A}(z) = \frac{|\Phi'|^2}{2\bar{U}^2} \frac{\alpha^2 + 3l^2}{\alpha^2 + l^2} + \frac{|\Phi|^2}{2\bar{U}^2}\left(\alpha^2 + \frac{3\bar{U}'^2}{\bar{U}^2}\right) - \frac{\bar{U}'(|\Phi|^2)'}{2\bar{U}^3}\frac{2\alpha^2 + 3l^2}{\alpha^2 + l^2},$$

$$\mathbb{B}(z) = \frac{\alpha^2}{2(\alpha^2 + l^2)}\left(\frac{|\Phi|^2}{\bar{U}^2}\right)',$$

$$\mathbb{C}(z) = -\frac{\alpha^2\Phi^*}{\bar{U}} + \frac{\alpha^2\bar{U}'}{\bar{U}(\alpha^2 + l^2)}\left(\frac{\Phi^*}{\bar{U}}\right)',$$

$$\mathbb{D}(z) = \frac{-\alpha^2}{\alpha^2 + l^2}\left(\frac{\Phi^*}{\bar{U}}\right)',$$

where * denotes complex conjugation.

Thus, given the primary Eulerian-mean shear flow $\bar{U}(z)$, the primary wave-field eigenfunction $\Phi(z)$ and appropriate boundary conditions (see §3), the eigenvalue problem for σ_1 is completely specified by the coupled system (2.3) and (2.7) together with (2.6) and (2.8).

3. Free surface and other boundary conditions

Equations (2.3) and (2.7) each require boundary conditions at $z = [z_a, z_b]$. Here we identify $z = z_b = 0$ with the mean free surface and locate z_a some distance below it. Since one equation is averaged and the other not it is tempting to derive these conditions independently from GLM and E. But doing so is unwise, because nonlinearities resulting from the product of two variables harmonic in x can realize an x-independent component that may be overlooked. Instead we invoke no average and employ only E; we then allow the boundary conditions to split into x-independent and x-dependent parts. Further, for reasons outlined below, it is prudent to carry out the analysis using straightforward ϵ, Δ and $\epsilon\Delta$ scaling given in (3.1), reverting to the more complicated CLg scaling (*vis-à-vis* (2.1)) at the end.

We thus begin by decomposing the Eulerian velocity $\boldsymbol{u}(x, y, z, t)$ as

$$\boldsymbol{u} = \boldsymbol{U} + \tilde{\boldsymbol{u}} + \breve{\boldsymbol{u}} = \boldsymbol{U}(z) + \epsilon\boldsymbol{U}_1(x, z, t) + \Delta\boldsymbol{u}_2(y, z, t) + \epsilon\Delta\boldsymbol{u}_3(x, y, z, t) \qquad (3.1)$$

where, as in §2.1, $\boldsymbol{U} = [U, 0, 0]$ is the imposed mean flow, $\tilde{\boldsymbol{u}} = \Delta\boldsymbol{u}_2$ is the velocity perturbation due to the instability and $\breve{\boldsymbol{u}} = \epsilon\boldsymbol{U}_1 + \epsilon\Delta\boldsymbol{u}_3$ is the primary and modulated wave field (cf. (2.4)). Note that although $\boldsymbol{u}_2$ may in general vary with x the variation is probably on a scale long with respect to the wavelength of the waves and so we assume, as in §2, that it is x-independent.

Our presumption is that there is a depth at which the wave field and velocity perturbations vanish, so we require that

$$\boldsymbol{U}_1 \to 0, \quad \boldsymbol{u}_1 \to 0 \quad \text{and} \quad \boldsymbol{u}_3 \to 0 \quad \text{as} \quad z \to -\infty. \qquad (3.2)$$

Boundary conditions at the free surface $z = 0$ were derived by PW, but they are restricted by the requirement that $l^2 \gg \alpha^2$, which necessitates that $\boldsymbol{u}_2 = 0$. Of course $\boldsymbol{u}_2$ need not in general be zero, so we shall now derive conditions which reflect that.

Appropriate boundary conditions are (the kinematic condition) that the free surface be a material surface of the fluid and (the dynamic condition) that there be continuity of pressure $\rho\mathscr{C}^2\mathfrak{p}$ (where ρ is density) at the surface. But because our wave field is rotational we cannot employ the Bernoulli form of E to derive the dynamic condition.

Instead we must require, in the absence of surface tension and with the position of the free surface given by $z = \eta(x, y, t)$, that

$$\frac{D(z-\eta)}{Dt} = 0 \quad \text{and} \quad \frac{D\boldsymbol{u}}{Dt} = -\nabla\mathfrak{p} + \boldsymbol{k}\mathfrak{g} \quad \text{on} \quad z = \eta, \qquad (3.3a, b)$$

noting that $\nabla\mathfrak{p}$ has no component lying along the free surface. Then $\nabla\mathfrak{p}$ is along the vector $\nabla(z - \eta)$, so that

$$\nabla\mathfrak{p} = \frac{\partial\mathfrak{p}}{\partial z}\nabla(z - \eta) \quad \text{on} \quad z = \eta.$$

Taylor's theorem may then be used to express $\nabla\mathfrak{p}$ on $z = \eta$ in terms of variables on $z = 0$.

Now the liquid surface is planar in the undisturbed state (so $\eta = 0$), the velocity field is $\boldsymbol{u} = [U, 0, 0]$ and the pressure is specified by the hydrostatic law $\mathfrak{p} = -\mathfrak{g}z$, where $\mathscr{C}^2\mathfrak{g}/\mathscr{L}$ is gravity. But when small, time-dependent three-dimensional perturbations are present, the free surface moves to $z = \eta$, thereby introducing an excess pressure at all z. In order to determine this pressure and ascertain boundary conditions at each order, we first expand $\mathfrak{p}$ and η in accord with (3.1), as

$$\mathfrak{p} = \mathscr{P}_0(z) + \epsilon\mathscr{P}_1(x, z, t) + \Delta\mathfrak{p}_2(y, z, t) + \epsilon\Delta\mathfrak{p}_3(x, y, z, t) + O(\epsilon\Delta^2) \qquad (3.4a)$$

and

$$\eta = N_0 + \epsilon N_1(x, t) + \Delta\eta_2(y, t) + \epsilon\Delta\eta_3(x, y, t) + O(\epsilon^2\Delta, \epsilon\Delta^2). \qquad (3.4b)$$

On substituting (3.1) and (3.4) into (3.3) our next task is to cast the expansion, at each order, in a form commensurate with the eigenvalue problem in §2; this requires that each variable be written in separable form. The form for $\boldsymbol{U}_1$ and $\boldsymbol{u}_3$ follows immediately from (2.4), albeit with x replaced by $X = x - \mathscr{C}t/\mathscr{C}$, but at $O(\Delta)$ we assume

$$\boldsymbol{u}_2 = \text{Re}\{e^{\sigma t}[\mathfrak{u}(z)\cos ly, \mathfrak{v}(z)\sin ly, \mathfrak{w}(z)\cos ly]\} + O(\epsilon^2, \epsilon\Delta^2). \qquad (3.5)$$

Finally we write

$$N_0 = \text{Re}\{\mathfrak{b}_0\}, \quad N_1 = \text{Re}\{\mathfrak{b}_1 e^{i\alpha X}\}, \qquad (3.6a, b)$$

$$\eta_2 = \text{Re}\{e^{\sigma t}\mathfrak{b}_2\cos ly\} \quad \text{and} \quad \eta_3 = \text{Re}\{e^{\sigma t}\mathfrak{b}_3 e^{i\alpha X}\cos ly\}, \qquad (3.6c, d)$$

where $\mathfrak{b}_i$ ($i = 0, 1, 2, 3$) are constants.

Looking first at $O(1)$, we find in accord with the non-perturbed state that $\mathscr{P}_0 = -\mathfrak{g}z$. We further see with no loss of generality that we may set $N_0 = 0$.

Turning now to $O(\epsilon)$ we see that the Rayleigh equation (2.5) follows from the x- and z-E equations, while eliminating N_1 from (3.3) yields the $O(\epsilon)$ free-surface boundary condition

$$\bar{U}^2\Phi' - (\bar{U}\bar{U}' + \mathfrak{g})\Phi = 0 \quad \text{on} \quad z = 0, \qquad (3.7)$$

with $\mathfrak{b}_1 = -\Phi(0)/\bar{U}$, while (3.2) requires at $O(\epsilon)$ that

$$\Phi \to 0 \quad \text{as} \quad z \to -\infty. \qquad (3.8)$$

Thus, given $\bar{U}$ and α, the velocity field $\alpha\Phi(z)$ of the wave is specified by (2.5) subject to (3.7) and (3.8).

Proceeding now to $O(\Delta)$, we find on $z = 0$ that

$$\sigma\mathfrak{u} + U'\mathfrak{w} = 0 \quad \text{and} \quad \sigma^2\mathfrak{w}' + l^2\mathfrak{g}\mathfrak{w} = 0. \qquad (3.9)$$

When written in terms of CLg scaling, however, where $\mathfrak{u} = \hat{u}$, $\mathfrak{w} = \epsilon\hat{w}$ and $\sigma = \epsilon\sigma_1$, we see that (3.9) is actually an $O(\epsilon\Delta)$ boundary condition as

$$\sigma_1\hat{u} + U'\hat{w} = 0 \quad \text{and} \quad \sigma_1^2\hat{w}' + l^2\mathfrak{g}\hat{w} = 0 \qquad (3.10a, b)$$

with $\mathfrak{b}_2 = \hat{w}(0)/\sigma_1$. Finally, since we solve for $\hat{u}$ (see §4) and since (3.10a) concurs with (2.3a), we may write (3.10) in terms of $\hat{u}$ as

$$\mathfrak{g}\hat{u} + \frac{\epsilon^2\sigma_1^2}{l^2}\left[\hat{u}' - \frac{U''}{U'}\hat{u}\right] = 0. \qquad (3.11)$$

Observe that (3.11) is a Cauchy boundary condition which reflects the fact that perturbation stresses may occur at the free surface.

Continuing then at $O(\epsilon\Delta)$, we first employ continuity to eliminate $\mathfrak{y}$ and $\mathfrak{y}$ from the x- and y-E equations. Then, since $\mathfrak{b}_1$ and $\mathfrak{b}_2$ are known and $\mathfrak{b}_3$ is given by substituting (3.6d) into (3.3a) we find after some algebra that our second $O(\epsilon\Delta)$ free-surface boundary condition is

$$\alpha^2\bar{U}\left[-\bar{U}\hat{\phi}' + U'\hat{\phi} + \Phi\hat{u}' + \left(\frac{\Phi\bar{U}l^2}{U'} - \Phi'\right)\hat{u}\right] + \mathfrak{g}(\alpha^2 + l^2)\left[\hat{\phi} - \frac{\Phi}{\bar{U}}\hat{u}\right]$$

$$+ \epsilon^2\sigma_1^2\left[-\hat{\phi}' + \frac{U'}{\bar{U}}\hat{\phi} + \frac{\Phi}{\bar{U}}\hat{u}' + \left((l^2 - \alpha^2)\frac{\Phi}{U'} - \frac{\Phi'}{\bar{U}}\right)\hat{u}\right] - \epsilon^4\sigma_1^4\frac{\Phi}{\bar{U}^2U'}\hat{u} = 0. \quad (3.12)$$

This boundary condition describes the level of wave distortion, or more precisely modifications $\alpha\hat{\phi}$ to the velocity field of the wave at the free surface $z = 0$ due to an $O(\Delta)$ axial velocity modification to the primary shear flow. We shall discuss (3.11) and (3.12) further in §3.1, but note here that the lead term of (3.12) recovers PW's counterpart boundary condition when $\hat{u} = 0$.

Lastly at large depth, and for consistency with (3.2), we require

$$\hat{u} \to 0, \quad \hat{\phi} \to 0 \quad \text{as} \quad z \to -\infty. \qquad (3.13a, b)$$

3.1. *Range of validity of the boundary conditions on $z = 0$*

Observe that although (3.11) is in general a Cauchy boundary condition, the second term vanishes when $\sigma_1 = O(1)$ and $\epsilon^2/l^2 \ll 1$, reducing (3.11) to the Dirichlet boundary condition $\hat{u} = 0$. However the second term cannot be ignored when $\epsilon^2/l^2 = O(1)$.

Equation (3.12) is also a Cauchy boundary condition. Indeed on writing (3.12) as

$$\alpha^2\bar{U}\left(1 + \frac{\epsilon^2\sigma_1^2}{\alpha^2\bar{U}^2}\right)\left[\left\{\left(1 - \frac{\epsilon^2\sigma_1^2}{l^2\bar{U}^2}\right)\frac{l^2\Phi\bar{U}}{U'} - \Phi'\right\}\hat{u} + \Phi\hat{u}' - \bar{U}\hat{\phi}' + U'\hat{\phi}\right]$$

$$+ \mathfrak{g}(\alpha^2 + l^2)\left(\hat{\phi} - \frac{\Phi}{\bar{U}}\hat{u}\right) = 0, \quad (3.14)$$

we see that the $O(\epsilon^2)$ terms must likewise be retained when $\epsilon^2/l^2 = O(1)$ and/or $\epsilon^2/\alpha^2 = O(1)$, although the $O(\epsilon^4)$ term is negligible provided $\epsilon^4/(\alpha^2 + l^2) \ll 1$. In consequence (3.11) and (3.12) are valid for $\epsilon^2/l^2 \leqslant O(1)$ and $\epsilon^2/\alpha^2 \leqslant O(1)$.

Looking now at the large-wavenumber limits, we first consider $\alpha^2 \gg l^2$. Here (3.14) becomes

$$\bar{U}\left[\left\{\left(1 - \frac{\epsilon^2\sigma_1^2}{l^2\bar{U}^2}\right)\frac{l^2\Phi\bar{U}}{U'} - \Phi'\right\}\hat{u} + \Phi\hat{u}' - \bar{U}\hat{\phi}' + U'\hat{\phi}\right] + \mathfrak{g}\left(\hat{\phi} - \frac{\Phi}{\bar{U}}\hat{u}\right) \sim 0,$$

which is independent of α and is thus uniformly valid for all $\alpha^2 \gg l^2$.

On the other hand (3.14) becomes

$$\alpha^2 \bar{U} \left(1 + \frac{\epsilon^2 \sigma_1^2}{\alpha^2 \bar{U}^2}\right) \left[\frac{\Phi \bar{U}}{U'} l^2 \hat{u} + \Phi \hat{u}' - \bar{U} \hat{\phi}' + U' \hat{\phi}\right] + \mathfrak{g} l^2 \left(\hat{\phi} - \frac{\Phi}{\bar{U}} \hat{u}\right) \sim 0$$

when $l^2 \gg \alpha^2$ and admits two distinguished limits: In the first $l^2 \hat{u} \neq 0$ when $l^2 \gg \alpha^2$ leaving

$$\alpha^2 \bar{U} \left(1 + \frac{\epsilon^2 \sigma_1^2}{\alpha^2 \bar{U}^2}\right) \frac{\Phi \bar{U}}{U'} \hat{u} + \mathfrak{g} \left(\hat{\phi} - \frac{\Phi}{\bar{U}} \hat{u}\right) \sim 0, \tag{3.15}$$

which is independent of l, indicating that (3.15) is uniformly valid for all $l^2 \gg \alpha^2$. Moreover because (3.11) necessitates that $\hat{u} \sim 0$ as $l^2 \to \infty$, we see that (3.15) likewise necessitates $\hat{\phi} \sim 0$, in accord with PW's rigid wall solution.

But if $l^2 \hat{u} \sim 0$ for some $l^2 \gg \alpha^2$, we find

$$\alpha^2 \bar{U} \left(1 + \frac{\epsilon^2 \sigma_1^2}{\alpha^2 \bar{U}^2}\right) \left[-\bar{U} \hat{\phi}' + U' \hat{\phi}\right] + \mathfrak{g} l^2 \hat{\phi} \sim 0, \tag{3.16}$$

which is not independent of l as $l^2 \to \infty$. This limit admits eigensolutions in which σ_1 increases with l for all $l^2 \gg \alpha^2$, rendering the linear eigenvalue problem ill-posed. Such behaviour is, of course, spurious and means that a correction term must enter at high wavenumber. Since our primary interest lies in the range of l for which (3.14) is valid, namely $\epsilon^2/l^2 \leqslant O(1)$ and $\epsilon^2 l^2 \leqslant O(1)$, we shall not seek a correction to (3.14) formally. Rather we observe that a high-wavenumber expansion in l probably results in a correction to the $\hat{\phi}'$ term, possibly as $\hat{\phi}'(1 + \epsilon^2 l^2)$, so that the second distinguished limit then becomes

$$\epsilon^2 \alpha^2 \bar{U} \left(1 + \frac{\epsilon^2 \sigma_1^2}{\alpha^2 \bar{U}^2}\right) l^2 \bar{U} \hat{\phi}' - \mathfrak{g} l^2 \left(\hat{\phi} - \frac{\Phi}{\bar{U}} \hat{u}\right) \sim 0, \tag{3.17}$$

which is independent of l and thereby ensures that the linear eigenvalue problem is well-posed. Finally, we shall see in §6 that (3.16) and (3.15) respectively describe upper- and lower-branch eigensolutions over some $l^2 \gg \alpha^2$ and that the upper branch is non-physical.

4. Numerical procedure

To recap, from E in the interior we have (2.7), subject to the boundary conditions (3.13b) on $z = z_a$ and (3.12) on $z = z_b$. Accordingly, after rewriting (2.3), we have from GLM in the interior that

$$\hat{u}'' + F \hat{u}' + G \hat{u} + \sigma_1^{-2} (H \hat{u} + I \hat{p}) = 0 \tag{4.1}$$

subject to the boundary conditions (3.13a) on $z = z_a$ and (3.11) on $z = z_b$. Here

$$F(z) = -\frac{2 \bar{U}''}{\bar{U}'}, \quad G(z) = 2 \left(\frac{\bar{U}''}{\bar{U}'}\right)^2 - \frac{\bar{U}'''}{\bar{U}'} - l^2, \quad H(z) = l^2 P' \bar{U}' \quad \text{and} \quad I(z) = -(l \bar{U}')^2.$$

We wish to solve for σ_1 directly for specified α, l and ϵ, noting that because (4.1) is real, the eigenvalues σ_1 may be real, imaginary or complex-conjugate pairs. In view of the complicated free-surface boundary conditions (3.11) and (3.12), we employ the tau-method. Here the functions $\hat{u}$ and $\hat{\phi}$ are expanded as

$$\hat{u}_N(z) = \sum_{i=1}^{N} b_i u_i(z) + b_{2N+1} \theta(z), \quad \hat{\phi}_N(z) = \sum_{i=1}^{N} b_{N+i} \phi_i(z) + b_{2N+2} \vartheta(z), \tag{4.2}$$

where u_i and ϕ_i are linearly independent complete sets of basis functions and θ and ϑ are arbitrary functions of z, while b_i are constants chosen to satisfy the differential equations (4.1) and (2.7), subject to the aforementioned boundary conditions. Substituting (4.2) into (2.7), (4.1) and using (2.8), then yields residuals for each equation; and requiring the residuals and each of the approximating functions to be orthogonal (see PW) leads to $2N$ of the required $2N + 2$ linear homogeneous algebraic equations for b_i. The remaining two equations arise from substitution into the free-surface boundary conditions on $z = z_b$, namely (3.12) and (3.13). In this instance, however, we do not take an inner product, rather we simply require the residual to be zero.

The ensuing $2N + 2$ equations for b_i can then be written in the form

$$\mathscr{L} = \sigma_1^{-2}\mathscr{M}, \tag{4.3}$$

where $\mathscr{L}$ and $\mathscr{M}$ are composed of matrix blocks with entries given by the inner products and residuals, for example

$$(L_{11})_{ij} = \langle u_i, (\mathrm{M} + F\mathrm{D} + G)u_j \rangle \quad \text{and} \quad (M_{12})_{ij} = \langle u_i, I\mathrm{Re}\{(\mathbb{C} + \mathbb{D}\mathrm{D})\phi_j\}\rangle,$$

where $\mathrm{D} \equiv \mathrm{d}/\mathrm{d}z$ and $\mathrm{M} \equiv \mathrm{d}^2/\mathrm{d}z^2$. Non-zero solutions to (4.3) exist only if the determinant of the coefficients vanishes, i.e.

$$\det(\mathscr{L} - \sigma_1^{-2}\mathscr{M}) = 0 \tag{4.4}$$

and, because (4.4) is a $2N + 2$-order polynomial equation, our expansion produces the first $2N + 2$ among the infinite number of eigenvalues of the system (4.3). Usually of interest for each pair $(\alpha, l; \epsilon)$ is the eigenvalue σ_1 with the largest real part and the associated eigenfunctions $\hat{u}$ and $\hat{\phi}$.

In our study with water of finite depth $z = z_a$, we set $z_b = 0$ and introduce the mapping $\zeta^* = 1 - z/z_a$ to ensure $[\zeta_a^*, \zeta_b^*] = [0, 1]$. Shifted Chebyshev polynomials were used as basis functions. When considering flow in water of infinite depth, on the other hand, we map from the semi-infinite $(z_a, z_b] = (-\infty, 0]$ to the finite plane with the mapping $\zeta = \mathrm{e}^z$, so that again $[\zeta_a, \zeta_b] = [0, 1]$. However in order to ensure that our perturbation quantities decay exponentially fast in z (as they must on physical grounds, Phillips (1996)), we likewise replace our dependent variables as, for example, $\hat{u} \mapsto \mathrm{e}^{\gamma z}\hat{u}$. Failure to satisfy this requirement can cause fallacious results owing to spurious singular behaviour arising from the truncation of the basis functions at finite N (Spalart, Moser & Rogers 1991). In this setting our operators become

$$\mathrm{D} \mapsto \mathrm{D}_\infty \equiv \zeta\frac{\mathrm{d}}{\mathrm{d}\zeta} + \gamma \quad \text{and} \quad \mathrm{M} \mapsto \mathrm{M}_\infty \equiv \zeta\frac{\mathrm{d}}{\mathrm{d}\zeta}\left(\zeta\frac{\mathrm{d}}{\mathrm{d}\zeta}\right) + 2\gamma\zeta\frac{\mathrm{d}}{\mathrm{d}\zeta} + \gamma^2,$$

although we here follow Phillips (2001b, 2002) and set $\gamma = 1$.

All computations were performed with double-precision arithmetic using Gaussian quadrature to evaluate the inner products, with LaPak routines to solve the eigenvalue problem. The accuracy provided by $N = 30$ was sufficiently accurate for most calculations, although to ensure mode-independent behaviour, some runs were done with successively higher N, to $N > 100$. An obvious test case was to repeat the calculations (both cases) of PW (herein with a new code): in all cases our numerical values closely recovered those of PW, although we note that the curves PW plot for growth rate with distortion (in their figures 1 and 4) are in fact for the case $\mathbb{C} = \mathbb{D} = 0$; the actual curves, as $\alpha \to 0$, fall below those drawn.

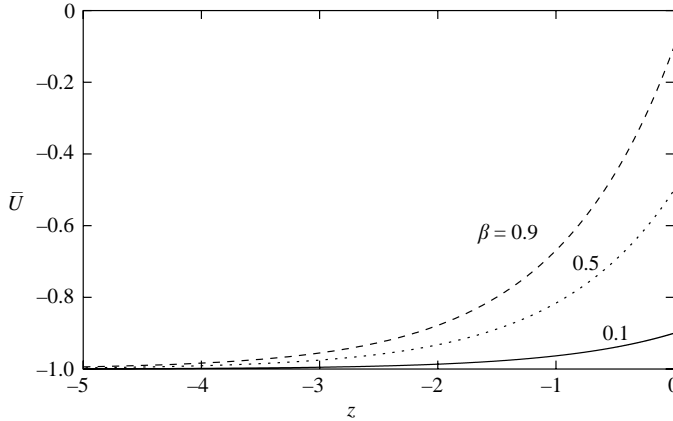FIGURE 1. Eulerian mean velocity $\bar{U}$ as a function of depth z for $\beta = 0.1, 0.5, 0.9$ and $h = 1$. Curves for negative β are obtained by adding 2 to their positive-β counterparts.

5. Primary velocity and wave fields

Following PW, we consider spanwise-independent $O(\epsilon)$ surface gravity waves in the presence of a unidirectional shear layer whose velocity profile $U(z)$ decreases with depth from the mean free surface $z = 0$, such that

$$\mathscr{C}\bar{U} = \mathscr{C}(\beta e^{hz} - 1) \quad (h > 0) \quad \text{over} - \infty < z \leqslant 0. \tag{5.1}$$

Then since $\beta = U(0)/\mathscr{C}$, and $\mathscr{C}$ may be of either sign, we require $\beta < 1$ to avoid critical layers; further, to conform with our scaling, we must limit $\beta = O(1)$. Profiles of $\bar{U}$ for several values of β are drawn in figure 1.

With $\bar{U}(z)$ known, we now return to the length scale $\mathscr{L}$ (used to render spatial variables dimensionless) and define it as the e-folding depth of the shear layer. Then, since $hz = -1$ and $\mathscr{L}z = -\mathscr{L}$ must occur concurrently in (5.1), we require $h = 1$.

Admissible primary wave fields follow from (5.1) and (2.5) subject to the boundary conditions (3.7) and (3.8) which lead directly to (see PW)

$$\alpha\phi = \gamma\zeta^{\alpha}F(a, b; c; \zeta) \quad \text{for} \quad \zeta \in [0, \beta]. \tag{5.2}$$

Here $\zeta = \beta e^{z}$ and $F(a, b; c; \zeta)$ is the hypergeometric series (Abramowitz & Stegun 1964), in which

$$a = \alpha + (\alpha^2 + 1)^{1/2}, \quad b = \alpha - (\alpha^2 + 1)^{1/2} \quad \text{and} \quad c = 1 + 2\alpha.$$

Straightforward analysis then yields the product $\bar{u}'P'$ (see PW); profiles of P for several values of $\pm\beta$ are drawn in figure 2.

6. Langmuir circulations in water of finite and infinite depth

6.1. *Background*

We first revisit the problem considered by PW in which the wavy shear flow is described by (5.1) and (5.2), and the depth is specified by the e-folding depth of the shear. Unlike PW, however, who allowed anomalies in the mean flow and subsequent modulation of the wave field in the interior only, we allow anomalies both in the interior and at the free surface, but not at the base. To be specific, we place the mean free surface at $z_b = 0$ and the base at $z_a = -1$ with boundary conditions as specified in
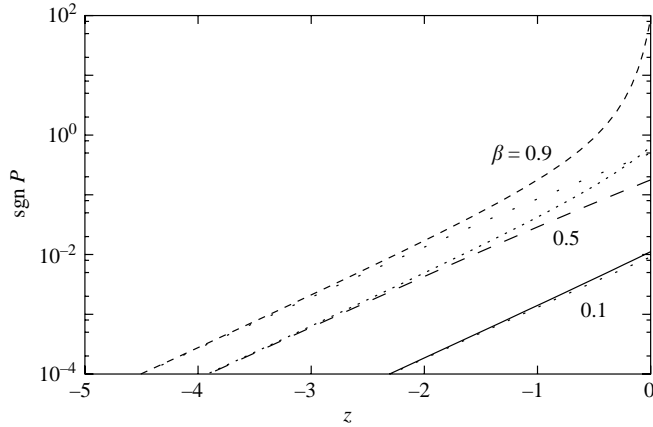
FIGURE 2. Primary pseudomomentum P as a function of depth z for $\alpha = 1$ and $\pm\beta = 0.1, 0.5, 0.9$ with $h = 1$. In each instance the lower curve is for negative β. Note that the sign of P is determined by the sign of $-\bar{U}$.
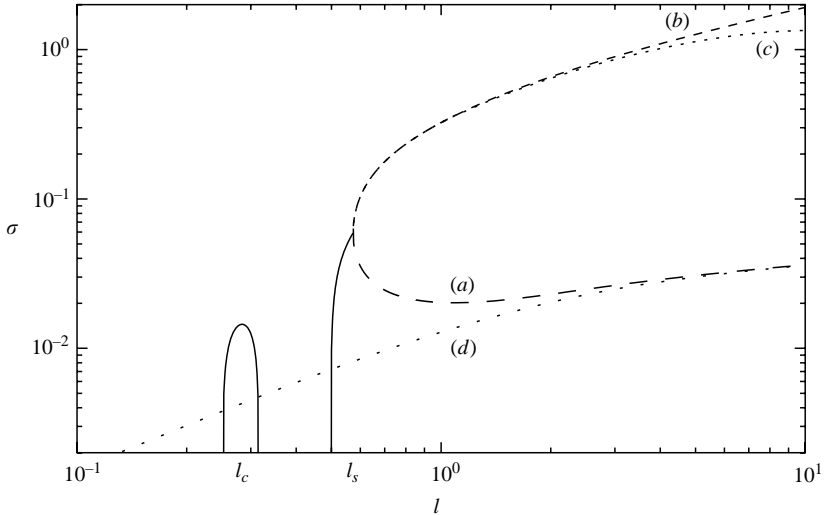

FIGURE 3. Comparison of the real part of the maximum growth rate $\sigma = \epsilon\sigma_1$ as a function of l for $\epsilon = 0.1$, $\alpha = 1$, $\beta = 0.5$ and $z_a = -1$: $(a\text{--}c)$ with a free surface; (a) with (3.14) asymptotic to the distinguished limit (3.15); (b) with (3.14) asymptotic to the distinguished limit (3.16); (c) with (3.14) asymptotic to the regularized distinguished limit (3.17); (d) with rigid boundaries (from Phillips & Wu 1994).

§ 3. Then because P is non-zero at $z_a = -1$ (see figure 2), the base is necessarily wavy. The flow then models that in an open channel with a rigid wavy bottom, or in the ocean mixed layer bounded from below by a wavy non-deformable pycnocline. PW found that wave modulation acts to diminish the instability, at least for sufficiently large l or sufficiently small α. They also found that the maximum growth rate is, in each case, given by an eigenvalue that is purely real.

6.2. *Results*

Consider first the real part of the growth rate $\sigma = \epsilon\sigma_1$ as a function of the spanwise wavenumber l (figure 3) with, for comparison, PW's result (with wave modulation)
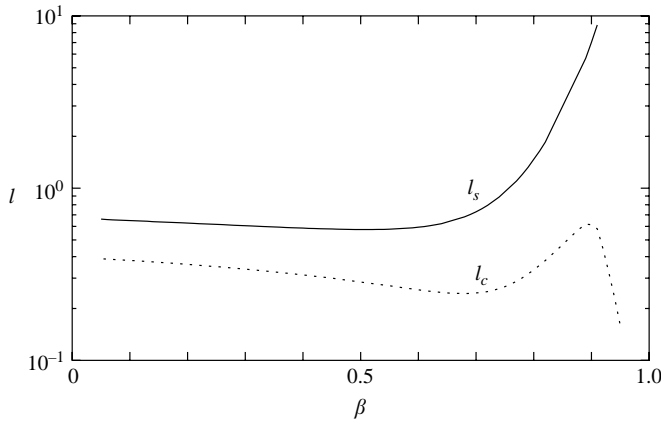
FIGURE 4. Trace of the preferred wavenumbers l_s and l_c against β for $\epsilon = 0.1$, $\alpha = 1$ and $z_a = -1$.

with rigid boundaries. Observe the presence of a narrow peak near $l = l_c \approx 0.28$. Here the eigenvalues appear as complex-conjugate pairs suggesting that the LC are born in an oscillatory convective mode. Further, since the band of instability exhibits a local maximum at l_c it is evident that l_c is a preferred spacing. Instability resumes once $l > 0.5$, also with complex eigenvalues. Rather than mimic its predecessor, however, this branch undergoes a Hopf bifurcation at $l = l_s \approx 0.58$ to form upper (*b*, *c*) and lower (*a*) eigenbranches on which the eigenvalues are purely real. The lower branch is asymptotic to PW's solution (*d*), while the upper branch is asymptotic to the respective distinguished limits (3.16) (*b*) or (3.17) (*c*), the latter including a high-wavenumber correction. The free-surface perturbations $\hat{u}$ and $\hat{\phi}$ together approach zero (as $l \to \infty$) on the lower branch (see §3.1), but not on the upper, where $\hat{\phi}$ can remain non-zero with $\hat{u}$ zero. Such behaviour is, of course, non-physical because $\hat{u}$ causes $\hat{\phi}$, and our inclination is to discard the upper branch. That said, the linear eigenspectrum is complete only with both branches and both must be retained as initial conditions in the nonlinear problem. Growth along both branches is also likely when solving the nonlinear problem, at least initially. Ultimately, however, nonlinearities typically damp out growth from the high-growth (upper) non-physical branch (see e.g. Short 1997) causing the solution to lock onto the lower branch. Should this be the case here, we are then left with two preferred spanwise wavenumbers, l_s where LC is born in a stationary bifurcation and l_c, where LC originates in an oscillatory convective mode.

6.3. *Preferred spacing and the role of α and β*

We now question the affect of α and β on l_s, l_c noting that, in view of our normalization, the streamwise wavenumber α is also a measure of whether the surface waves are long or short with respect to the e-folding depth of the shear. Our findings are plotted in figures 4, 5, 6 and 7. We begin by fixing α and varying β, noting that our eigenvalue problem was posed under the assumption that $\beta = O(1)$, subject to the caveat that $\beta < 1$. Observe that l_s remains larger than l_c (figure 4) and that the the growth rate associated with l_s is, at least for $\beta < 0.9$, significantly larger than that for l_c (figure 5). Thus l_s is probably the more robust of the two spacings and so we plot it as a function of α in figure 6. Here we see that l_s increases significantly with β and that, except for $\beta = 0.9$, diminishes with increasing $\alpha > 1$. To gain further insight into the behaviour with α, we plot in figure 7 growth rate against α at two
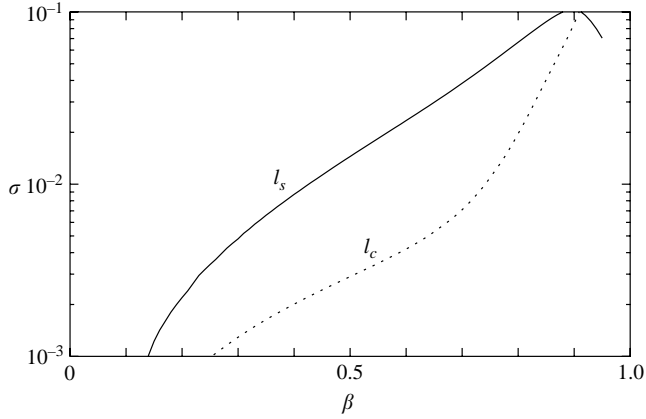
FIGURE 5. Growth rate $\sigma = \epsilon\sigma_1$ at the preferred wavenumbers l_s and l_c against β for $\epsilon = 0.1$, $\alpha = 1$ and $z_a = -1$.
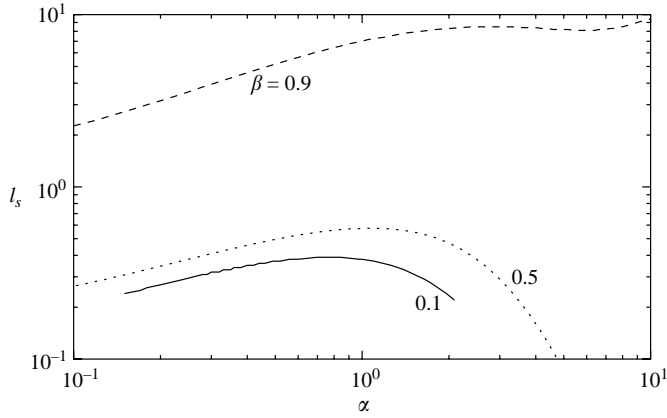

FIGURE 6. Trace of the preferred wavenumbers l_s of the instability as a function of α for $\epsilon = 0.1$ and $\beta = 0.1, 0.5, 0.9$ for $z_a = -1$.
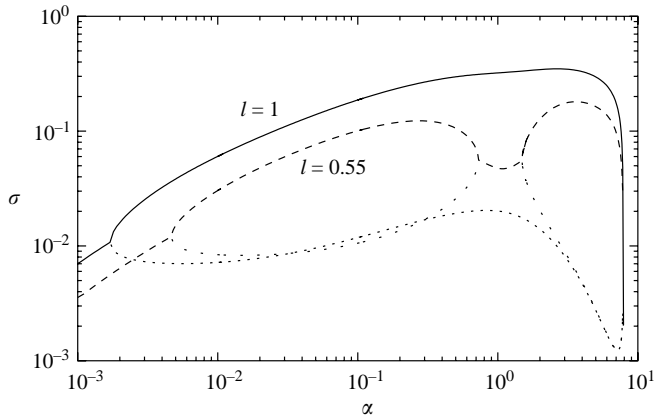

FIGURE 7. Growth rate $\sigma = \epsilon\sigma_1$ against α for $\epsilon = 0.1$ and $\beta = 0.5$ when $l = 0.55$ and $l = 1$ with $z_a = -1$.
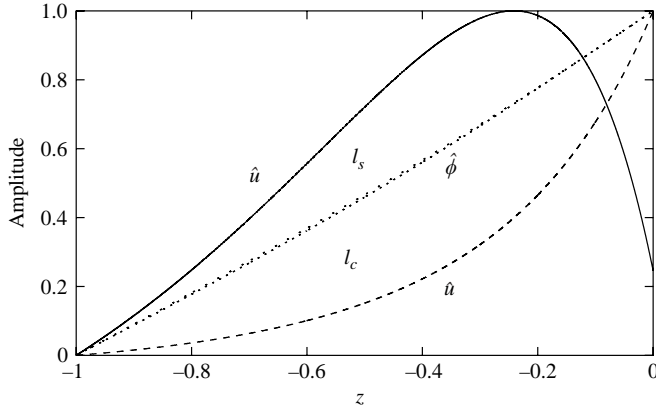
FIGURE 8. Perturbation eigenfunctions $\hat{u}$ and $\hat{\phi}$ at $l_c = 0.28$ and $l_s = 0.57$ with $\epsilon = 0.1$, $\alpha = 1$, $\beta = 0.5$ and $z_a = -1$.
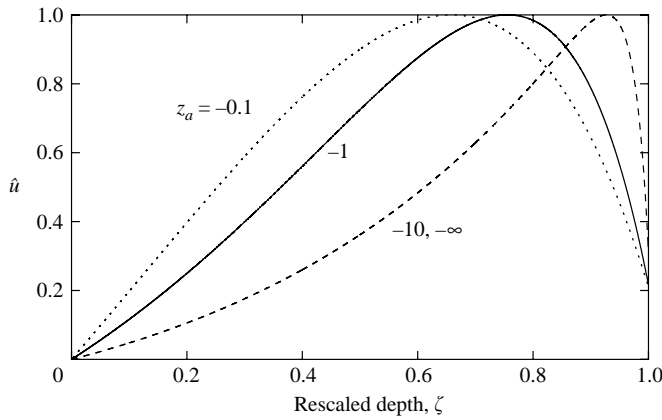

FIGURE 9. Perturbation eigenfunctions $\hat{u}$ at l_s with $\epsilon = 0.1$, $\alpha = 1$ and $\beta = 0.5$ for various depths $-z_a = 0.1, 1, 10, \infty$.

values of l. Here we find that the upper and lower branches reconnect at about $\alpha = 8$ to depict a high-streamwise-wavenumber cutoff.

6.4. *Eigenfunctions and the role of α and β*

Eigenfunctions for $\hat{u}$ and $\hat{\phi}$ are drawn in figures 8, 9 and 10. Those shown are for $\alpha = 1$ and $\beta = 0.5$ but they are representative of a much broader range of α and β. Observe in figure 8 that while the eigenfunctions for $\hat{u}$ and $\hat{\phi}$ are a maximum at the free surface and decrease with depth at l_c, that is not the case at l_s where $\hat{u}$ is a maximum below the surface. This feature is reflected at all depths as we see in figure 9, whereas $\hat{\phi}$ is always a maximum at the free surface ($\zeta = 1$), figure 10.

6.5. *Langmuir circulation in water of various depths*

We now vary the depth of the water from significantly less than the shear layer e-folding depth, to vastly greater than it. Specifically, we set the mean free surface at $z_a = 0$ and vary z_a from $-z_a \in [0.1, \infty)$. The results are given in figures 9 to 13 and figure 16, all of which include results for $z_a = -1$ as reference.

Looking first at the infinite depth result in figure 11, we see that the preferred wavenumber l_s increases almost monotonically with α, whereas it in shallow water it
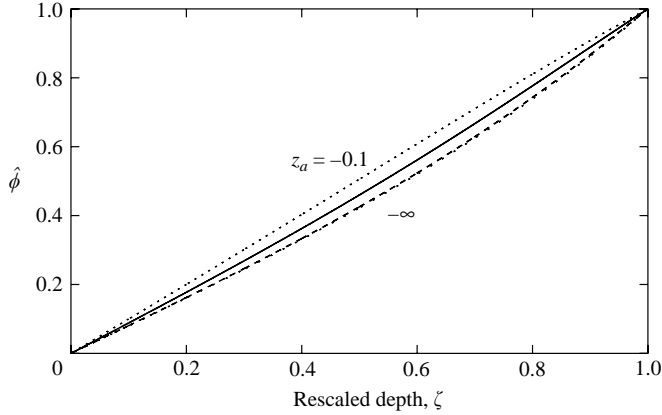
FIGURE 10. Perturbation eigenfunctions $\hat{\phi}$ at l_s with $\epsilon = 0.1$, $\alpha = 1$ and $\beta = 0.5$ for various depths $-z_a = 0.1, 1, 10, \infty$.
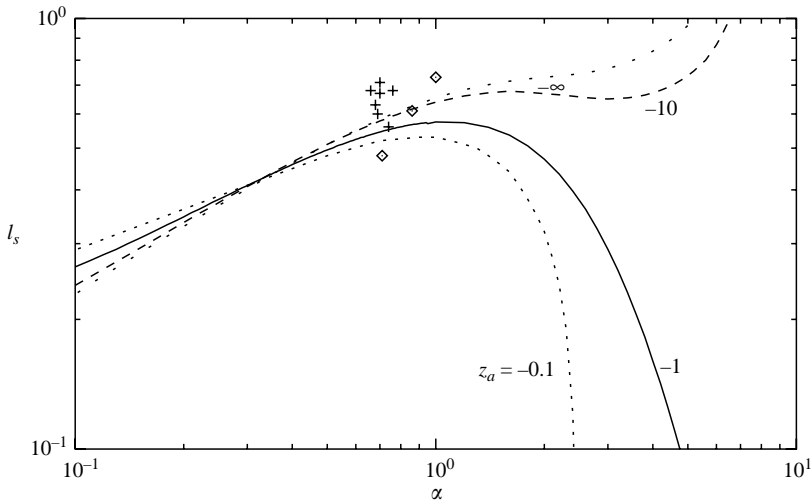

FIGURE 11. Trace of the preferred wavenumber l_s against α at various depths: $-z_a = 0.1, 1, 10, \infty$ for $\beta = 0.5$ and $\epsilon = 0.1$. $\diamond$, Data of Melville *et al.* (1998); $+$, data of Veron & Melville (2001).

falls rapidly once $\alpha > 1$. The ratio of α/l_s is plotted against α in figure 12 and here we observe only a minor variation with depth for $\alpha < 1$. Plotted also are the data of Melville *et al.* (1998) and Veron & Melville (2001) which we see concur well with the calculations. However, since the data clump around $\alpha \approx 0.7$ on this plot we next plot (figure 13) l_c and l_s against β (with $\alpha = 0.7$) at various depths. Observe that the data best concur with l_s, the preferred spacing with the highest growth rate. Note also that depth has little influence on l_s, at least for $\beta < 0.6$. Finally, note that the preferred mode l_c occurs only for a small range of β near $\beta \approx 0.9$ as $z_a \to \infty$ and is thus absent in figure 13.

6.6. *The role of wave slope*

Finally we turn to the role of wave slope ϵ. Wave slope is absent in the equations of motion but features in the boundary conditions (3.11) and (3.12), ostensibly for $(\epsilon/l)^2 = O(1)$. We see in figures 14 and 15 that both l_s and σ increase with ϵ. We
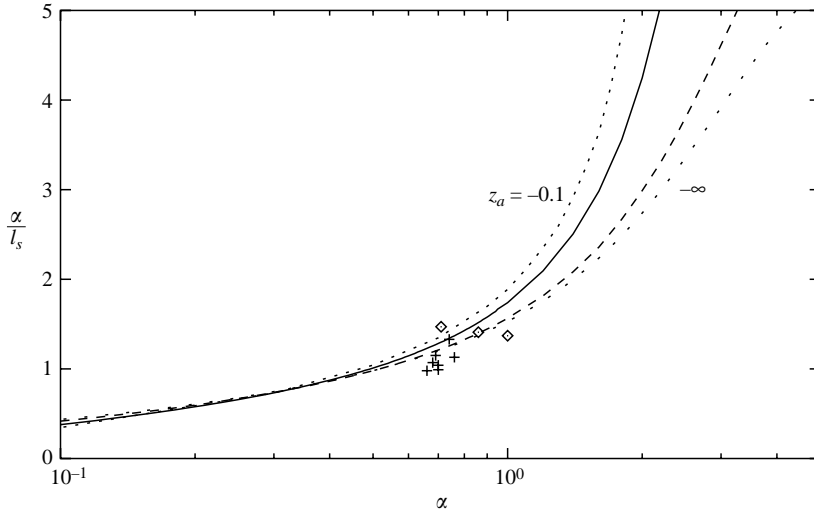
FIGURE 12. Streamwise wavenumber α normalized by the preferred wavenumber l_s as a function of α at various depths: $z_a = -0.1, -1, -10$ and $z \to -\infty$ for $\beta = 0.5$ and $\epsilon = 0.1$. $\diamond$, Data of Melville *et al.* (1998); $+$, data of Veron & Melville (2001).
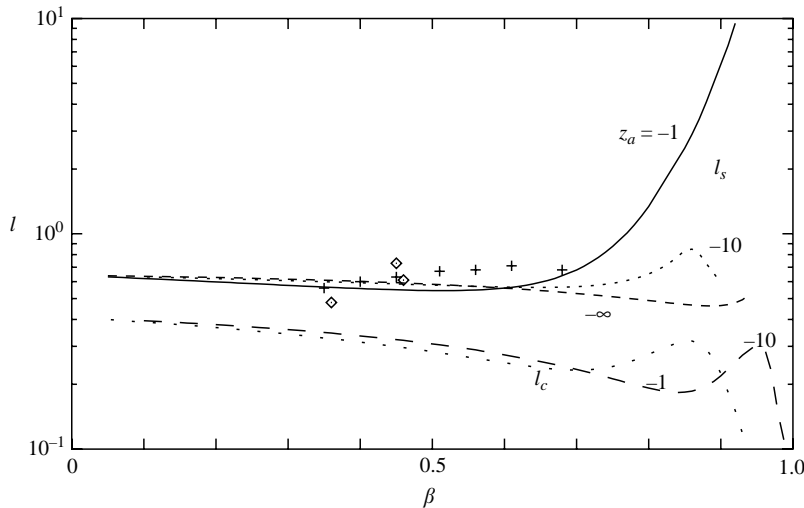

FIGURE 13. Trace of the preferred wavenumbers l_s and l_s of the instability as a function of β for $\epsilon = 0.1$ and $\alpha = 0.7$ for depths $-z_a = 1, 10, \infty$. $\diamond$, Data of Melville *et al.* (1998); $+$, data of Veron & Melville (2001).

further see in figure 16 that growth rate increases linearly (asymptotically) with ϵ, as assumed in our scaling. The same figure also suggests that there is also a strong depth dependence, with the highest growth rate occurring in shallow water.

7. Comparison with experiment

7.1. *Data reduction*

In order to compare our findings with the experimental data it is necessary to first normalize them in the manner employed herein. So, since our spatial scales are
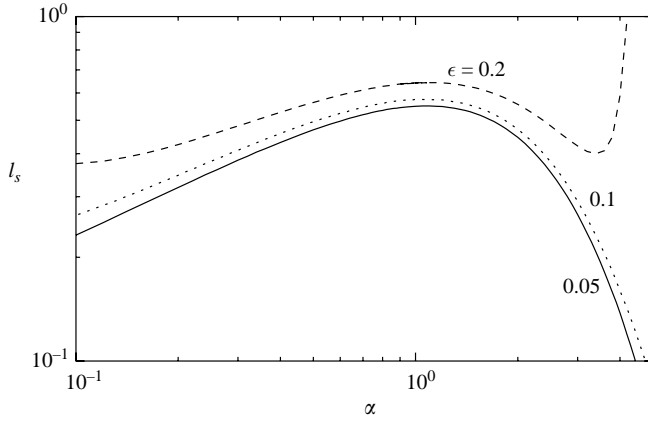
FIGURE 14. Trace of the preferred wavenumber l_s against α for various wave slopes: $\epsilon = 0.05, 0.1, 0.2$ for $\beta = 0.5$ and $z_a = -1$.
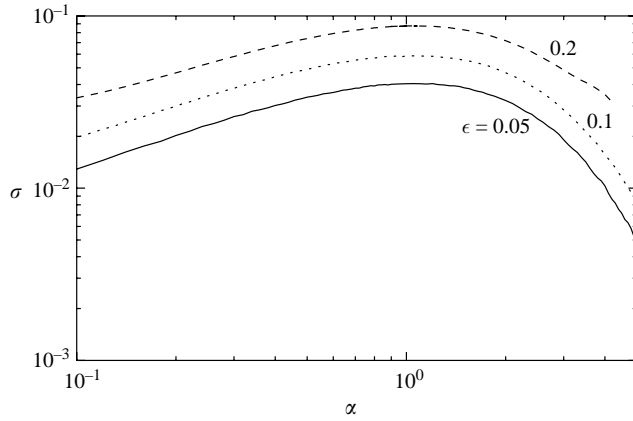

FIGURE 15. Trace of the growth rate $\sigma = \epsilon\sigma_1$ at the preferred wavenumber l_s for various wave slopes: $\epsilon = 0.05, 0.1, 0.2$ for $\beta = 0.5$ and $z_a = -1$.
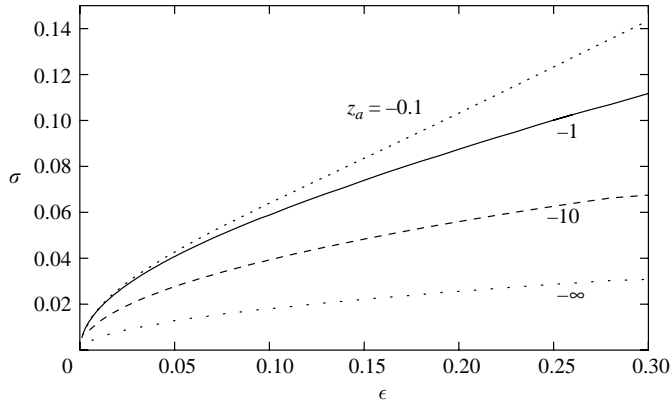

FIGURE 16. Variation in the growth rate $\sigma = \epsilon\sigma_1$ at l_s against wave slope for $\alpha = 1$, $\beta = 0.5$ at various depths, $-z_a = 0.1, 1, 10, \infty$.

Wind speed (m s^{-1})	Time (s)	$\mathscr{L}$ (cm)	α	l	β	$\mathfrak{g}$	Time (s)	$\mathscr{L}$ (cm)	α	l	β	$\mathfrak{g}$
3.0	52	0.58	0.71	0.48	0.36	0.48	40	0.51	0.74	0.56	0.35	0.63
3.5							33	0.46	0.69	0.60	0.40	0.58
4.0	34	0.47	0.86	0.61	0.46	0.49	27	0.42	0.68	0.63	0.45	0.56
4.5							22	0.38	0.70	0.67	0.51	0.55
5.0	23	0.38	1.00	0.73	0.45	0.23	18	0.34	0.66	0.68	0.56	0.51
5.5							16	0.32	0.70	0.71	0.61	0.51
6.0							13	0.29	0.76	0.68	0.68	0.50

TABLE 1. Values of the e-folding depth $\mathscr{L}$ (see §5.2), the wavenumbers α and l, the shear ratio β and a gravitational measure $\mathfrak{g}$ for Melville *et al.*'s (1998) data (left) and Veron & Melville's (2001) data (right).

normalized by the depth at which the velocity falls to e^{-1} of its surface value, we seek a representative value of $\mathscr{L}$ for each wind speed used in Melville *et al.*'s (1998) and Veron & Melville's (2001) experiments. This we obtain from the similarity solution given by Melville *et al.*, which is seen to be a good approximation to the data (see their figure 13*a*). In particular, since the similarity solution suggests that the e-folding depth occurs near $z^*/(2(\nu t^*)^{1/2}) \approx -0.4$, we set $\mathscr{L} = 0.8(\nu t^*)^{1/2}$ and use it with $\nu = 1.0 \times 10^{-6}$ m s^{-1} to determine values of α, l and β, which are given in table 1.

7.2. *Primary flow*

Accordingly, before comparing our instability results with their experimental counterparts, it is necessary to ensure that our primary flow credibly reflects that in the experiment; for this we employ the gravitational measure $\mathfrak{g}$. Bear in mind that we do not specify $\mathfrak{g}$ directly; rather we specify β (which defines $\bar{U}$ through (5.1)) and α (which defines Φ through (2.5)), which together define $\mathfrak{g}$ through the $O(\epsilon)$ free-surface boundary condition (3.7). In the simplest case we could plot $\mathfrak{g}$ as a function of β for various values of α, but $\mathfrak{g}$ is unbounded in α and we prefer a dependent variable composed of $\mathfrak{g}$ and α that is bounded. To proceed therefore we note, from (2.5) and (3.7), that $\mathfrak{g}$ varies from α when $\beta = 0$ to zero when $\beta = 1$, the former case depicting linear waves in deep water (in the absence of capillary effects and shear), as it must since $\mathfrak{g} = g\mathscr{L}/\mathscr{C}^2$ (see §3). So to ensure boundedness we introduce the dependent variable $\mathfrak{g}/\alpha$, and plot it, in figure 17, as a function of β for various α in the range considered in §6. Observe that $\mathfrak{g}/\alpha$ diminishes monotonically with increasing β and that its sensitivity to α diminishes with increasing α. Note too that $\mathfrak{g}/\alpha$ is essentially a Froude number based upon wave speed $\mathscr{C}$ and dimensional wavenumber $\alpha/\mathscr{L}$.

Plotted also on figure 17 are Melville *et al.*'s (1998) and Veron & Melville's (2001) experimental results listed in table 1. Veron & Melville's data, whose average α is about 0.7, also diminish with β, but lie above our curve for $\alpha = 0.7$; in fact they lie close to our curve for $\alpha = 0.1$. Melville *et al.*'s data, on the other hand, at least two of their three points, are numerically closer to our results. Of course we do not expect a one-to-one correspondence here; all we require is that Froude numbers for the theory and data be subcritical and within an order of magnitude of each other, and thankfully that is the case. In short our primary flow does credibly reflect that in the experiment and so it is meaningful to compare our instability results with those observed experimentally.
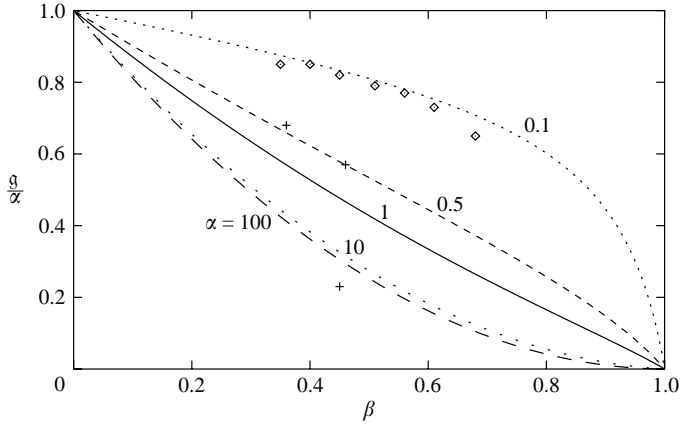
FIGURE 17. Plot of $\mathfrak{g}/\alpha$ against β for various values of α. $+$ Data of Melville *et al.* (1998); $\diamond$ data of Veron & Melville (2001).

7.3. *Secondary flow*

Melville *et al.*'s and Veron & Melville's data are plotted in figures 11, 12 and 13. The first two figures show preferred spanwise wavenumber l_s against α at various depths, while β is varied with α fixed in figure 13. In each instance the data are remarkably close to our calculation for the fastest growing preferred spacing l_s. The same is true in figure 12, where we plot α/l_s, a ratio easily determined from observations, against α. In consequence, we conclude that the instability exciting LC in the experiment is very likely to be CLg.

8. Discussion

Our study of the CLg instability in strong wavy shear with a free surface indicates that wave modulation due to current anomalies acts in concert with the free surface to set the cross-wind spacing both for the anomalies and for the Langmuir circulation. The process is inviscid and the instability is in accord with the Craik–Phillips–Shen criterion, although unlike the rigid wall case, where wave modulation acts to diminish the instability, it here enhances it, at least for some spanwise wavenumbers. Features of particular interest are that, while preferred spacing is only weakly dependent upon the depth of the water for $\alpha < 1$ (figure 11) it is dependent on the level of shear (figure 5). Moreover, while the LC is single layered in deep and shallow water (figure 9), the maximum streamwise velocity anomaly is not always at the free surface (figures 8 and 9). Wave distortion, on the other hand, is always a maximum at the free surface (figure 10).

Comparison with the experimental data of Melville *et al.* (1998) and Veron & Melville (2001), shows that our preferred cross-wind spacings occurring in a stationary bifurcation concur well with their observations, and it appears highly likely that the instability mechanism exciting Langmuir circulations in their experiments is CLg. This means that the CLg instability is physically realizable not only in the presence of rigid wavy walls (Phillips *et al.* 1996), but also beneath deformable surface gravity waves.

Of particular interest, of course, is whether CL2, which is a degenerate case of CLg in $O(\epsilon^2)$ shear, is by default also physically realizable. Certainly differential drift is key in each case, but whereas a free surface here acts in concert with wave modulation to set the cross-wind spacing, there is no such counterpart in CL2. Indeed the free

surface is rigid in CL2 and the fastest growing mode given by inviscid linear stability analysis occurs when $l \to \infty$ (Leibovich 1977). In contrast ocean LC would appear to have a preferred spacing (see for example figure 7 in Smith 1992) and it is prudent to question whether it too is set by wave modulation, at least partially.

In considering the notion we should bear in mind that the term which reflects wave modulation (the right-hand side of (2.3b)) is premultiplied by ϵ^s in CLg (see equation (4.1b) in Phillips 1998). We further note that the level of shear associated with the dominant-slope waves in the open ocean is $O(\epsilon^2)$, for which $s = 2$. Thus, either wave modulation is negligible as assumed in CL2, or the scaling employed in constructing the CLg equations is inappropriate for levels of shear $s > 0$. On the other hand LC are known to form in a variety of levels of shear in the open ocean (Melville *et al.*), which brings to mind a scenario put forward by Phillips *et al.* (1999) and reinforced by Phillips (2001b). Specifically that ocean LC originates in the strong shear ($s = 0$) regime and then grow in scale (spanwise) as they cascade through medium ($s = 1$) to ultimately weak shear, only to be sustained by the dominant-slope waves.

If we take this notion further, an immediate question is whether the ratio of the streamwise to spanwise wavelengths at which LC first form (in $O(1)$ shear) is robust to subsequent diminution in shear, and the answer would appear to be yes. Consider, for example, Smith's ocean observations where, over a three hour time frame, α/l_s increases (see his figure 7) from approximately 0.4 to 2.5, values that are well within the range depicted in figure 12 for values of $\alpha \in (0.1, 2)$. Since the dominant-slope waves have a wavelength of about 25 m, then $\mathcal{L} \approx 25\alpha/2\pi \approx 4\alpha$ m and we can use our results to estimate e-folding depths in the ocean. Indeed, our $z_a = -1$ curve suggests $\mathcal{L} \in (0.4\,\text{m}, 6\,\text{m})$, while our $z_a = -10$ curve suggests $\mathcal{L} \in (0.4\,\text{m}, 7\,\text{m})$ and our infinite depth curve suggests $\mathcal{L} \in (0.4\,\text{m}, 8\,\text{m})$. The results are striking, first because we expect $\mathcal{L}$ to be less than the mixed layer depth and it is, as is evident from plate 4 in Smith (1992). Here we see that the mixed layer depth increases, after the onset of LC, from about 10 m to 20 m. Second, $\mathcal{L}$ should not be at odds with estimates given by $0.8(\nu_T t^*)^{1/2}$, where ν_T is now an eddy viscosity and t^* is the time after a marked increase in wind velocity. Indeed, using the value $\nu_T = 0.025$ m^2 s^{-1} employed by Phillips' (2001b) in another comparison with Smith's observations, we find a characteristic depth of 4 m after fifteen minutes (the t^* at which LC were first observed), 8 m after one hour and 13 m after three hours.

REFERENCES

ABRAMOWITZ, M. & STEGUN, I. A. 1964 *Handbook of Mathematical Functions*. Dover.

ANDREWS, D. G. & MCINTYRE, M. E. 1978 An exact theory of nonlinear waves on a Lagrangian-mean flow. *J. Fluid Mech.* **89**, 609–646.

CRAIK, A. D. D. 1982 Wave-induced longitudinal-vortex instability in shear layers. *J. Fluid Mech.* **125**, 37–52.

CRAIK, A. D. D. & LEIBOVICH, S. 1976 A rational model for Langmuir circulations, *J. Fluid Mech.* **73**, 401–426.

GONG, W., TAYLOR, P. A. & DÖRNBRACK, A. 1996 Turbulent boundary-layer flow over fixed, aerodynamically rough two-dimensional sinusoidal waves. *J. Fluid Mech.* **312**, 1–37.

LANGMUIR, I. 1938 Surface motion of water induced by wind. *Science* **87**, 119–123.

LEIBOVICH, S. 1977 Convective instability of stably stratified water in the ocean. *J. Fluid Mech.* **82**, 561–585.

McINTYRE, M. E. 1988 A note on the divergence effect and the Lagrangian-mean surface elevation in periodic water waves. *J. Fluid Mech.* **189**, 235–242.

McINTYRE, M. E. & NORTON, W. A. 1990 Dissipative wave-mean interactions and the transport of vorticity or potential vorticity. *J. Fluid Mech.* **212**, 403–435.

MELVILLE, W. K., SHEAR, R. & VERON, F. 1998 Laboratory measurements of the generation and evolution of Langmuir circulations. *J. Fluid Mech.* **364**, 31–58.

PHILLIPS, W. R. C. 1996 On a class of unsteady boundary layers of finite extent *J. Fluid Mech.* **319**, 151–170.

PHILLIPS, W. R. C. 1998 Finite amplitude rotational waves in viscous shear flows. *Stud. Appl. Maths* **101**, 23–47.

PHILLIPS, W. R. C. 2001*a* On the pseudomomentum and generalized Stokes drift in a spectrum of rotational waves. *J. Fluid Mech.* **430**, 209–229.

PHILLIPS, W. R. C. 2001*b* On an instability to Langmuir circulations and the role of Prandtl and Richardson numbers. *J. Fluid Mech.* **442**, 335–358.

PHILLIPS, W. R. C. 2002 Langmuir circulations beneath growing or decaying surface waves. *J. Fluid Mech.* **469**, 317–342.

PHILLIPS, W. R. C. 2003 Langmuir circulations. In *Wind-Over-Waves II: Forecasting and Fundamentals of Applications* (ed S. G. Sajjadi & J. C. R. Hunt), pp. 157–167. Horwood.

PHILLIPS, W. R. C. & SHEN, Q. 1996 A family of wave-mean shear interactions and their instability to longitudinal vortex form. *Stud. Appl. Maths* **96**, 143–161.

PHILLIPS, W. R. C. & WU, Z. 1994 On the instability of wave-catalysed longitudinal vortices in strong shear. *J. Fluid Mech.* **272**, 235–254 (referred to herein as PW).

PHILLIPS, W. R. C., WU, Z. & JAHNKE, C. C. 1999 Longitudinal vortices in wavy boundary layers. In *Wind-Over-Wave Couplings: Perspectives and Prospects* (ed. S. G. Sajjadi, N. H. Thomas, & J. C. R. Hunt), pp. 41–47. Oxford University Press.

PHILLIPS, W. R. C., WU, Z. & LUMLEY, J. L. 1996 On the formation of longitudinal vortices in turbulent boundary layers over wavy terrain. *J. Fluid Mech.* **326**, 321–341.

SHORT, M. 1997 A parabolic linear evolution equation for cellular detonation instability. *Combust. Theor. Mod.* **1**, 313–346.

SMITH, J. A. 1992 Observed growth of Langmuir circulation *J. Geophys. Res.* **97**, 5651–5664.

SPALART, P. R., MOSER, R. D. & ROGERS, M. M. 1991 Spectral methods for the Navier-Stokes equations with one infinite and two periodic directions. *J. Comput. Phys.* **96**, 297–324.

THORPE, S. A. 2004 Langmuir circulation. *Annu. Rev. Fluid Mech.* **36**, 55–79.

VERON, F. & MELVILLE, W. K. 2001 Experiments on the stability and transition of wind-driven water surfaces. *J. Fluid Mech.* **446**, 25–65.